Nano-Hz Gravitational-Wave Signature from Axion Dark Matter

Naoya Kitajima,[1,2,*] Jiro Soda,[3,†] and Yuko Urakawa[4,5,‡]
[1]Frontier Research Institute for Interdisciplinary Sciences, Tohoku University, Sendai 980-8578, Japan
[2]Department of Physics, Tohoku University, Sendai 980-8578, Japan
[3]Department of Physics, Kobe University, Kobe 657-8501, Japan
[4]Department of Physics and Astrophysics, Nagoya University, Chikusa, Nagoya 464-8602, Japan
[5]Fakultät für Physik, Universität Bielefeld, 33501 Bielefeld, Germany

(Received 31 October 2020; accepted 23 February 2021; published 26 March 2021)

We calculate the accurate spectrum of the stochastic gravitational-wave background from U(1) gauge fields produced by axion dark matter. The explosive production of gauge fields soon invalidates the applicability of the linear analysis and one needs nonlinear schemes. We make use of numerical lattice simulations to properly follow the nonlinear dynamics such as backreaction and rescattering which gives important contributions to the emission of gravitational waves. It turns out that the axion with the decay constant $f \sim 10^{16}$ GeV and the mass $m \sim 10^{-14}$ eV which gives the correct dark matter abundance predicts the circularly polarized gravitational-wave signature detectable by SKA. We also show that the resulting gravitational-wave spectrum has a potential to explain NANOGrav 12.5 yr data.

DOI: 10.1103/PhysRevLett.126.121301

Introduction.—The cosmological observations have uncovered the existence of invisible matter known as dark matter. An axion, originally proposed to solve the strong *CP* problem [1–4] and later explored in a more general paradigm [5,6], is a candidate of dark matter [7–9]. To identify dark matter as an axion among various candidates, we need to look for its unique signature. Recently, the NANOGrav 12.5-yr data [10] reported a potential signal of a new physics. One may wonder if it is a hint of axion dark matter. In this Letter, we explore the possibility that axion dark matter can be searched from a measurement of nano-Hertz (nHz) gravitational waves (GWs) through pulsar timing observations such as PPTA [11], NANOGrav [12], and EPTA [13]. In the next decades, SKA [14] is expected to measure the GWs with an increased precision by several orders of magnitude.

The axion with a nonzero initial misalignment starts to oscillate, when the Hubble parameter becomes comparable to the mass, behaving as dark matter. Around the commencement of the oscillation, the U(1) gauge fields can be explosively produced through the coupling with the axion [15,16], leading to the emission of sizable amount of stochastic GWs as studied in Refs. [17–21]. [The GW emission from the U(1) gauge field production has also been studied in the gauge preheating scenario [22–24] and the decaying ultralight scalar model [25]. This mechanism is also applicable to generate primordial magnetic field [15,26–29], to reduce the abundance of QCD axion [30,31] and provide the correct relic abundance of the dark photon dark matter [32–34]].

In this Letter, conducing the numerical lattice simulation, which properly solves the nonlinear dynamics of the gauge fields and the axion, we show that the axion with the decay constant $f \sim 10^{16}$ GeV and the mass $m \sim 10^{-14}$ eV can generate the nHz GWs detectable by SKA while consistently explaining the dark matter abundance. (The nHz GWs can also be predicted by the decay of topological defects [35] and the scalar field fragmentation [36] in the axion dark matter scenario.) In addition, it also turns out that the resultant GW spectrum exhibits asymmetry between the two circular polarization modes as a characteristic signature of this scenario. The reported NANOGrav 12.5 yr data can also be explained in this scenario if one requires a drastic suppression for the relic axion density.

Gauge field production from axions.—Let us consider the interacting system of an axion (ϕ) and massless U(1) gauge fields (A_μ). The Lagrangian density is given by

$$\mathcal{L} = -\frac{1}{2}\partial^\mu\phi\partial_\mu\phi - V(\phi) - \frac{1}{4}F^{\mu\nu}F_{\mu\nu} - \frac{\alpha}{4f}\phi F_{\mu\nu}\tilde{F}^{\mu\nu}, \quad (1)$$

where $F_{\mu\nu} = \partial_\mu A_\nu - \partial_\nu A_\mu$ is the field strength tensor, $\tilde{F}^{\mu\nu} = \epsilon^{\mu\nu\rho\sigma}F_{\rho\sigma}/(2\sqrt{-g})$ is its dual with g being the determinant of the metric, α is a dimensionless coupling constant, and f is the decay constant of the axion. We consider the potential of the axion $V(\phi)$ given by

$$V(\phi) = \Lambda^4\left[1 - \cos\left(\frac{\phi}{f}\right)\right], \quad (2)$$

where Λ is a dynamical scale, which relates the axion mass m to the decay constant as $m = \Lambda^2/f$.

In what follows, we assume the radiation-dominated flat-FRW universe as the background spacetime with the scale

factor $a(t) \propto t^{1/2}$. The equation of motion for the axion is given by

$$\ddot{\phi} + 3H\dot{\phi} - \frac{1}{a^2}\nabla^2\phi + \frac{\partial V}{\partial \phi} = -\frac{\alpha}{4f} F_{\mu\nu}\tilde{F}^{\mu\nu}, \tag{3}$$

with the Hubble parameter $H = \dot{a}/a$. The overdot denotes the time derivative. The variation of the action with respect to A_0 yields the constraint equation (modified Gauss's law)

$$\partial_i \dot{A}_i - \frac{\alpha}{fa}\epsilon_{ijk}\partial_i\phi\partial_j A_k = 0, \tag{4}$$

and that with respect to A_i leads to the evolution equation of the gauge fields,

$$\ddot{A}_i + H\dot{A}_i - \frac{1}{a^2}\nabla^2 A_i + \frac{1}{a^2}\partial_i\partial_j A_j = \frac{\alpha}{fa}\epsilon_{ijk}(\dot{\phi}\partial_j A_k - \partial_j\phi\dot{A}_k), \tag{5}$$

where we have chosen the temporal gauge, $A_0 = 0$. We assume that the axion is homogeneously produced by misalignment mechanism with initial angle $\theta_i = \phi_i/f$ which is set before or during inflation. (In general, the initial value of the axion fluctuates but such initial fluctuations, as long as they are sufficiently small, do not affect the dynamics of the gauge fields since the self-resonance is inefficient in the cosine potential case [37,38].)

As shown below, the interaction with the axion amplifies the gauge fields exponentially. Although the axion can interact with the standard model photon, the photon acquires a thermal effective mass in the Universe filled with charged particles, which is much larger than the Hubble parameter, i.e., the axion mass at the onset of the oscillation. In that case, the gauge field production is kinematically prohibited. Therefore, we assume that the gauge fields are hidden photons which are not thermalized at the onset of the axion oscillation.

To see the exponential growth, let us decompose the Fourier mode of the gauge fields into two circular polarization modes as $\mathbf{A}(\mathbf{k}, t) = A_+(\mathbf{k}, t)\mathbf{e}^+(\mathbf{k}) + A_-(\mathbf{k}, t)\mathbf{e}^-(\mathbf{k})$ with the circular polarization bases, which satisfy $\hat{\mathbf{k}} \cdot \mathbf{e}^\pm = 0$ and $i\hat{\mathbf{k}} \times \mathbf{e}^\pm = \pm\mathbf{e}^\pm$ with $\hat{\mathbf{k}} \equiv \mathbf{k}/|\mathbf{k}|$. In the linear approximation, the axion is assumed to be homogeneous in the equation of motion for the gauge fields. In this case, the dynamics of each circular polarization mode is determined by the following equation of motion,

$$\ddot{A}_\pm + H\dot{A}_\pm + \left(\frac{k^2}{a^2} \mp \frac{k}{a}\frac{\alpha\dot{\phi}}{f}\right)A_\pm = 0. \tag{6}$$

This equation implies that, depending on the sign of $\dot{\phi}$, one of the two circular polarization modes can be tachyonic, leading to the exponential amplification of the gauge field amplitude.

Nonlinear dynamics.—Once the tachyonic instability turns on, the gauge fields grow exponentially and the energy density of the gauge fields eventually becomes comparable to that of the axion. Then the gauge field production is saturated and the linear approximation is broken down. In particular, the produced gauge fields start to affect the axion dynamics through the right-hand side in Eq. (3), producing inhomogeneous modes of the axion. After that, the two polarization modes no longer evolve independently, but they are mixed through the interaction with nonzero mode axions. In addition, the subsequent rescattering process significantly modifies the momentum distributions of both the axion and the gauge fields. Therefore, one needs to solve the nonlinear dynamics of the system to accurately compute the GW sources and the relic axion abundance.

We have directly solved Eqs. (3) and (5) by performing lattice simulations which enable us to analyze accurately the fully nonlinear dynamics. We adopted the second order Leapfrog method for the integration scheme. Both the axion and the gauge fields are treated as variables on each grid point. (See Ref. [32] for details.) The number of grid points is 256^3 and the comoving box size is $(\pi/2)m^{-1}$ for $\alpha = 18$ or $(\pi/4)m^{-1}$ for $\alpha = 20, 25, 30$. Figure 1 shows the evolution of the energy density of the axion, ρ_ϕ, and the gauge fields, ρ_A, in terms of the scale factor divided by the one at the onset of the axion oscillation, defined by $H = m$. The figure shows that the growth of the gauge fields terminates when its energy density catches up that of the axion, namely $a/a_{\rm osc} \simeq 15$ for $\alpha = 30$, which implies that the dynamics enters the nonlinear regime after that.

Figure 2 shows the evolution of the comoving number density spectrum of the gauge fields after the gauge field production is saturated. The spectrum has a sharp peak soon after the saturation, i.e., at $a/a_{\rm osc} = 16$, but it is broaden and flatten as time goes on. It is nothing but the consequence of the nonlinear dynamics. As a result, the

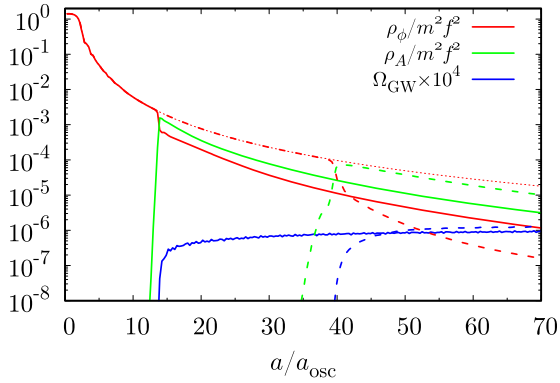

FIG. 1. The evolution of the energy density of the axion (red), the gauge fields (green), $\Omega_{\rm GW} \times 10^4$ (blue), and the adiabatic evolution of the axion without gauge field production (thin dotted red). We have taken $f = 10^{16}$ GeV, $m = 2 \times 10^{-14}$ eV, $\theta_i = 2$ and $\alpha = 30$ (solid) and 18 (dashed).

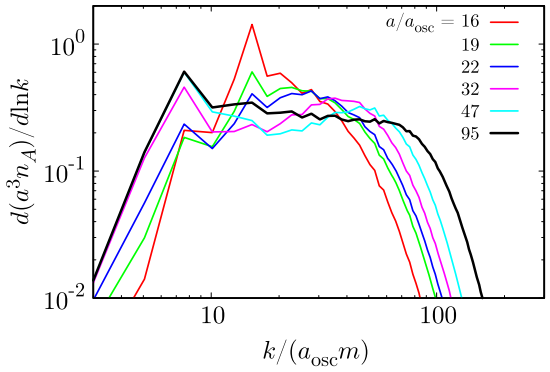

FIG. 2. The evolution of the spectrum of comoving number density of the gauge fields (a^3n_A) after the saturation normalized by $a_{\rm osc}^3mf^2$. We have taken $f = 10^{16}$ GeV, $m = 2 \times 10^{-14}$ eV, $\theta_i = 2$, and $\alpha = 30$.

spectrum is significantly deformed from the one at the saturation, implying the significant departure from the one obtained by the linear analysis.

Figure 3 shows the α dependence of the resultant comoving number density spectra of the gauge fields and the axion. For $\alpha = 18$, the sharp peak is kept in the spectrum, indicating that the nonlinear effect is not so efficient. On the other hand, the spectrum was significantly deformed through the nonlinear effect for $\alpha \geq 20$. Meanwhile, we have found that for $\alpha \leq 17$, the growth of the gauge fields stops before the saturation due to the cosmic expansion. The threshold value changes for different choices of f, m, and θ_i.

Relic axion dark matter abundance.—Figure 1 also shows that the axion energy density drops suddenly at the saturation, leading to the suppression of the relic axion abundance compared to the case without gauge field production. The suppression factor ϵ can be as small as $\sim 10^{-2}$, as also pointed out in Ref. [31] in the QCD axion case. Thus, we obtain the relic axion abundance at present as

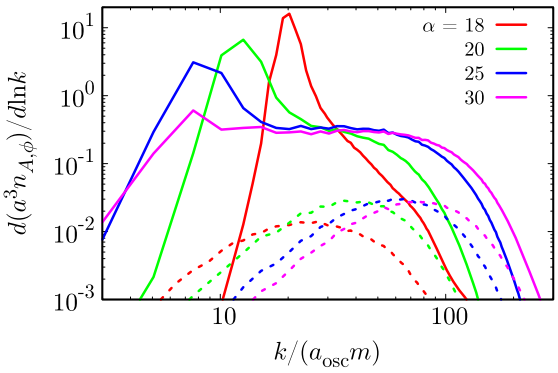

FIG. 3. The α dependence of the resultant spectra of the comoving number density of the gauge fields (a^3n_A, solid) and the axion (a^3n_ϕ, dashed) normalized by $a_{\rm osc}^3mf^2$. We have taken $f = 10^{16}$ GeV, $m = 2 \times 10^{-14}$ eV, $\theta_i = 2$, $\alpha = 18$ (red), 20 (green), 25 (blue), and 30 (magenta).

$$\Omega_a h^2 \sim 2.8\epsilon \left(\frac{g_{*\rm osc}}{10}\right)^{-1/4} \left(\frac{m}{10^{-14}\ \text{eV}}\right)^{1/2} \left(\frac{f\theta_i}{10^{16}\ \text{GeV}}\right)^2, \tag{7}$$

where, $g_{*\rm osc}$ is the effective relativistic degrees of freedom at the onset of the axion oscillation. Note that nonzero mode axions dominantly contribute to the abundance [31]. If a string axion with $f\theta_i \sim 10^{16}$ GeV accounts for the present dark matter component, the observed dark matter abundance determines the corresponding axion mass as $m \sim 10^{-14}$ eV for $\epsilon \sim 10^{-2}$. It should be noted that the simplest scenario explaining the dark matter abundance without gauge field production, i.e., $\epsilon = 1$ and thus $m \sim 10^{-17}$ eV for $f\theta_i \sim 10^{16}$ GeV, is excluded by the black hole spin measurements [39], while $m \sim 10^{-14}$ eV is within the allowed region.

Gravitational-wave emission.—The explosively generated gauge fields can source the stochastic background of GWs, which is given by the tensor component of the metric perturbation h_{ij}, defined in the background flat-FRW universe as follows

$$ds^2 = -dt^2 + a^2(\delta_{ij} + h_{ij})dx^i dx^j. \tag{8}$$

The perturbed Einstein equation for the tensor mode determines the evolution of the GWs,

$$\ddot{h}_{ij} + 3H\dot{h}_{ij} - \frac{1}{a^2}\nabla^2 h_{ij} = \frac{2}{M_P^2}\Pi_{ij}^{\rm TT}, \tag{9}$$

where $\Pi_{ij}^{\rm TT}$ is the transverse-traceless part of the anisotropic stress. In the system of our interest, the anisotropic stress is given by the traceless part of

$$\Pi_{ij} = -\frac{1}{a^2}\partial_i\phi\partial_j\phi + \frac{1}{a^2}E_iE_j + \frac{1}{a^2}B_iB_j. \tag{10}$$

where $E_i = \dot{A}_i$ and $B_i = \epsilon_{ijk}\partial_j A_k/a$ are, respectively, the electric and magnetic components of the gauge fields.

First, let us make a crude estimation of the peak amplitude of the GWs sourced by gauge fields or inhomogeneous axions which are amplified by the oscillating axion. Assuming for simplicity that the dominant fraction of the GWs is emitted around the saturation, the peak amplitude of the GW is roughly estimated as

$$\frac{k^2}{a_{\rm em}^2}h_{ij}(t_{\rm em}) \sim \frac{\rho_{\rm src}(t_{\rm em})}{M_P^2} \sim \left(\frac{mf\theta_i}{M_P}\right)^2 \left(\frac{a_{\rm osc}}{a_{\rm em}}\right)^3, \tag{11}$$

where $a_{\rm em}$ is the scale factor at the emission, $t = t_{\rm em}$, and $\rho_{\rm src}$ is the energy density of the source fields, which becomes comparable to the energy density of the homogeneous mode of the axion at $t_{\rm em}$. Then, one obtains the density parameter of the GW, $\Omega_{\rm GW} = M_P^2\langle\dot{h}_{ij}\dot{h}_{ij}\rangle/(4\rho_{\rm cr})$ (with the critical density $\rho_{\rm cr}$), at the emission as [40]

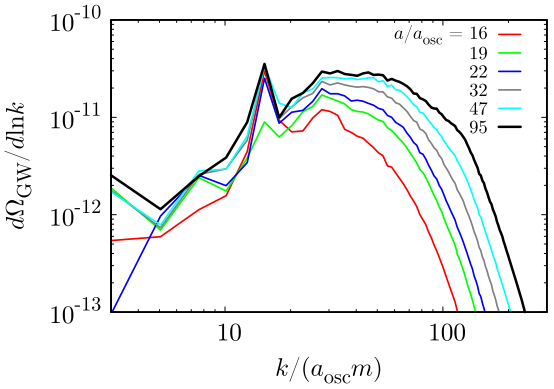

FIG. 4. The evolution of the spectrum of $\Omega_{\rm GW}$ after the saturation for the same setup as in Fig. 2.

$$\Omega_{\rm GW}(t_{\rm em}) \sim \left(\frac{k}{a_{\rm em}m}\right)^{-2}\left(\frac{f\theta_i}{M_P}\right)^4\left(\frac{a_{\rm osc}}{a_{\rm em}}\right)^2, \qquad (12)$$

and at present as $\Omega_{\rm GW}h^2 = \kappa\Omega_r h^2\Omega_{\rm GW}(t_{\rm em})$, where $\Omega_r h^2 \simeq 4.15\times10^{-5}$ is the present density parameter of radiation component and κ is given by $\kappa \simeq 1.8 g_{*\rm em}/g_{*S\,\rm em}^{4/3}$ with $g_{*\rm em}$ and $g_{*S\,\rm em}$ being the effective degrees of freedom in energy density and entropy density at the emission. Note that the typical wave number of emitted GWs is $k/a_{\rm em} \sim m$. For example, for $f = 10^{16}$ GeV, $\theta_i = 2$, $m = 2\times10^{-14}$ eV and $\alpha = 30$, we found $a_{\rm em}/a_{\rm osc} \simeq 15$ from Fig. 1 and then we obtain $\Omega_{\rm GW}(t_{\rm em}) \sim 2\times10^{-11}$ ($\Omega_{\rm GW}h^2 \sim 7\times10^{-16}$) which shows an acceptable agreement with the numerical result (see Figs. 4 and 5).

The GW frequency at present is related to the axion mass as follows [40,41]

$$\nu = \frac{k}{2\pi a_0} \sim 0.1\ {\rm nHz}\frac{g_{*\rm osc}^{1/4}}{g_{*S\rm osc}^{1/3}}\frac{k}{a_{\rm osc}m}\left(\frac{m}{10^{-14}\ {\rm eV}}\right)^{\frac{1}{2}}, \qquad (13)$$

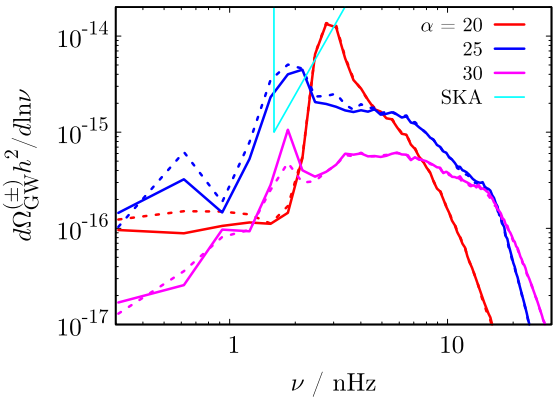

FIG. 5. The α dependence of the resultant spectrum of $\Omega_{\rm GW}h^2$ decomposed into two circular polarization modes, $\Omega_{\rm GW}^{(+)}h^2$ (solid line) and $\Omega_{\rm GW}^{(-)}h^2$ (dashed line). We have taken $f = 10^{16}$ GeV, $\theta_i = 2$, $m = 2\times10^{-14}$ eV, and $\alpha = 20$ (red), 25 (blue), 30 (magenta).

with a_0 the present scale factor and $g_{*S\rm osc}$ the effective relativistic degrees of freedom in entropy density at the onset of the axion oscillation. For $f \sim 10^{16}$ GeV, the axion with $m \sim 10^{-14}$ eV, which gives the observed dark matter abundance, predicts the GWs in nHz range with $\Omega_{\rm GW}h^2 \sim 10^{-15}$ for $a_{\rm osc}/a_{\rm em} = O(0.1)$.

As a result of the lattice simulation, the evolution of $\Omega_{\rm GW}$ is shown by the blue lines in Fig. 1. The generation of the GWs continues even after the saturation, being affected by the nonlinear dynamics of the gauge fields and the axion such as the rescattering. In particular, as shown in Fig. 4, which shows the evolution of the spectrum of $\Omega_{\rm GW}$, i.e., $d\Omega_{\rm GW}/d\ln k$, for $\alpha = 30$, the spectrum is broaden and the maximum amplitude becomes larger after the system enters the nonlinear regime. The former is because the spectrum of the gauge fields becomes broader as shown in Fig. 2. In most cases, compared to the numerical result, Eq. (12) underestimates the amount of GWs because the emission after the saturation is ignored.

Figure 5 shows the prediction of the present GW spectrum together with the sensitivity of SKA [14] in the case where the axion gives a consistent value with the observed dark matter abundance. Here, $\Omega_{\rm GW}^{(\pm)}$ denotes the contribution of either of two circular polarization modes to the total $\Omega_{\rm GW}$. Figure 5 indicates that the GWs from the axion dark matter are detectable by SKA, providing a new window for axion dark matter search. The spectrum has a sharp peak for $\alpha = 20$, and as α increases, the width of the spectrum becomes broader. Accordingly, the height of the spectrum drops by $\mathcal{O}(0.1)$. Therefore this model can predict both a highly peaked spectrum and a broadly extended spectrum depending on α.

Let us address whether the reported signal by NANOGrav [10] can be accounted for in this scenario. It requires $d\Omega_{\rm GW}h^2/d\ln\nu \sim 10^{-9}$ in nHz range. Since the density of emitted GWs roughly scales as $\Omega_{\rm GW} \propto f^4$ and $\Omega_{\rm GW} \sim 10^{-15}$–$10^{-14}$ for $f = 10^{16}$ GeV (see Fig. 5), one needs $f \sim 2$–4×10^{17} GeV to explain the NANOGrav data. In that case, however, the relic axion abundance becomes two or three orders of magnitude larger than the observed dark matter abundance. Then, one needs further suppression mechanism for this scenario to work with such a large decay constant.

As is shown in Fig. 5, this scenario predicts not only the detectable GW signal but also the circular polarization of the GW. Figure 6 shows the time evolution of the difference between two circular polarization modes of the density parameter of the GW and the energy density of the gauge fields. The predicted asymmetry of the circular polarization is 1%–10% depending on the coupling. It is possible in principle to detect the circular polarization with pulsar timing arrays by observing an anisotropy of GWs [42,43].

Discussion.—In this Letter, we focus only on the axion playing a role of the dark matter. Specifically, for the GUT scale decay constant, i.e., $f \sim 10^{16}$ GeV, our

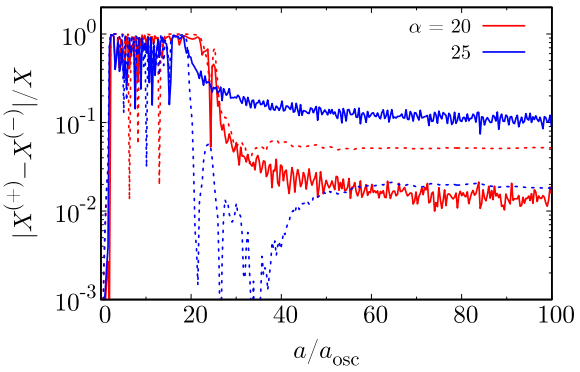

FIG. 6. The evolution of the circular polarization asymmetry for GWs ($X = \Omega_{\rm GW}$, solid lines) and gauge fields ($X = \rho_A$, dashed lines). We have taken $f = 10^{16}$ GeV, $\theta_i = 2$, $m = 2 \times 10^{-14}$ eV, and $\alpha = 20$ (red) and 25 (blue).

scenario predicts the axion mass $m \sim 10^{-14}$ eV and detectable nHz GWs. However, axions with different masses might exist in the context of the string axiverse. In that case, GWs in multifrequency bands can also be produced in the cosmological history, dubbed GW forest [40,41] (see also Refs. [17,44]). The frequency and the density parameter for GWs (emitted during radiation domination) are roughly given by Eqs. (13) and (12), respectively. Although axions in some mass ranges have to decay after the GW emission to avoid overproduction, the GW emission process for other frequency bands follows more or less the same story as the one in nHz band studied in this Letter, predicting the circularly polarized GW forest for a certain range of α. We leave such extensions for a future study.

We thank Wolfram Ratzinger and Pedro Schwaller for helpful comments. N. K. is supported by JSPS KAKENHI Grants No. JP18H01243, No. JP19K14708, and No. 20H01894. N. K. and Y. U. are supported by JSPS KAKENHI Grant No. JP19H01894. J. S. was in part supported by JSPS KAKENHI Grants No. JP17H02894 and No. JP20H01902. Y. U. is also supported by the Deutsche Forschungsgemeinschaft (DFG, German Research Foundation)—Project No. 315477589—TRR 211. The authors thank Yukawa Institute for Theoretical Physics at Kyoto University. Discussions during the YITP workshop YITP-T-19-02 on "Resonant instabilities in cosmology" were useful to complete this work.

*naoya.kitajima.c2@tohoku.ac.jp
†jiro@phys.sci.kobe-u.ac.jp
‡yuko@physik.uni-bielefeld.de

[1] R. D. Peccei and H. R. Quinn, Phys. Rev. Lett. **38**, 1440 (1977).
[2] R. D. Peccei and H. R. Quinn, Phys. Rev. D **16**, 1791 (1977).
[3] S. Weinberg, Phys. Rev. Lett. **40**, 223 (1978).
[4] F. Wilczek, Phys. Rev. Lett. **40**, 279 (1978).
[5] P. Svrcek and E. Witten, J. High Energy Phys. 06 (2006) 051.
[6] A. Arvanitaki, S. Dimopoulos, S. Dubovsky, N. Kaloper, and J. March-Russell, Phys. Rev. D **81**, 123530 (2010).
[7] J. Preskill, M. B. Wise, and F. Wilczek, Phys. Lett. **120B**, 127 (1983).
[8] L. Abbott and P. Sikivie, Phys. Lett. **120B**, 133 (1983).
[9] M. Dine and W. Fischler, Phys. Lett. **120B**, 137 (1983).
[10] Z. Arzoumanian *et al.* (NANOGrav Collaboration), Astrophys. J. Lett. **905**, L34 (2020).
[11] G. Hobbs, Classical Quantum Gravity **30**, 224007 (2013).
[12] Z. Arzoumanian *et al.* (NANOGRAV Collaboration), Astrophys. J. **859**, 47 (2018).
[13] L. Lentati *et al.*, Mon. Not. R. Astron. Soc. **453**, 2577 (2015).
[14] G. Janssen *et al.*, Proc. Sci. AASKA14 (**2015**) 037.
[15] W. D. Garretson, G. B. Field, and S. M. Carroll, Phys. Rev. D **46**, 5346 (1992).
[16] F. Finelli and A. Gruppuso, Phys. Lett. B **502**, 216 (2001).
[17] C. S. Machado, W. Ratzinger, P. Schwaller, and B. A. Stefanek, J. High Energy Phys. 01 (2019) 053.
[18] C. S. Machado, W. Ratzinger, P. Schwaller, and B. A. Stefanek, Phys. Rev. D **102**, 075033 (2020).
[19] B. Salehian, M. A. Gorji, S. Mukohyama, and H. Firouzjahi, arXiv:2007.08148.
[20] W. Ratzinger and P. Schwaller, arXiv:2009.11875.
[21] R. Namba and M. Suzuki, Phys. Rev. D **102**, 123527 (2020).
[22] P. Adshead, J. T. Giblin, and Z. J. Weiner, Phys. Rev. D **98**, 043525 (2018).
[23] P. Adshead, J. T. Giblin, M. Pieroni, and Z. J. Weiner, Phys. Rev. Lett. **124**, 171301 (2020).
[24] P. Adshead, J. T. Giblin, M. Pieroni, and Z. J. Weiner, Phys. Rev. D **101**, 083534 (2020).
[25] Z. J. Weiner, P. Adshead, and J. T. Giblin, Phys. Rev. D **103**, 021301 (2021).
[26] M. S. Turner and L. M. Widrow, Phys. Rev. D **37**, 2743 (1988).
[27] T. Fujita, R. Namba, Y. Tada, N. Takeda, and H. Tashiro, J. Cosmol. Astropart. Phys. 05 (2015) 054.
[28] P. Adshead, J. T. Giblin, T. R. Scully, and E. I. Sfakianakis, J. Cosmol. Astropart. Phys. 10 (2016) 039.
[29] T. Patel, H. Tashiro, and Y. Urakawa, J. Cosmol. Astropart. Phys. 01 (2020) 043.
[30] P. Agrawal, G. Marques-Tavares, and W. Xue, J. High Energy Phys. 03 (2018) 049.
[31] N. Kitajima, T. Sekiguchi, and F. Takahashi, Phys. Lett. B **781**, 684 (2018).
[32] P. Agrawal, N. Kitajima, M. Reece, T. Sekiguchi, and F. Takahashi, Phys. Lett. B **801**, 135136 (2020).
[33] R. T. Co, A. Pierce, Z. Zhang, and Y. Zhao, Phys. Rev. D **99**, 075002 (2019).
[34] M. Bastero-Gil, J. Santiago, L. Ubaldi, and R. Vega-Morales, J. Cosmol. Astropart. Phys. 04 (2019) 015.
[35] T. Higaki, K. S. Jeong, N. Kitajima, T. Sekiguchi, and F. Takahashi, J. High Energy Phys.08 (2016) 044.
[36] A. Chatrchyan and J. Jaeckel, J. Cosmol. Astropart. Phys. 02 (2021) 003.
[37] H. Fukunaga, N. Kitajima, and Y. Urakawa, J. Cosmol. Astropart. Phys. 06 (2019) 055.

[38] H. Fukunaga, N. Kitajima, and Y. Urakawa, J. Cosmol. Astropart. Phys. 02 (2021) 015.
[39] M. J. Stott, arXiv:2009.07206.
[40] N. Kitajima, J. Soda, and Y. Urakawa, J. Cosmol. Astropart. Phys. 10 (2018) 008.
[41] J. Soda and Y. Urakawa, Eur. Phys. J. C **78**, 779 (2018).
[42] R. Kato and J. Soda, Phys. Rev. D **93**, 062003 (2016).
[43] E. Belgacem and M. Kamionkowski, Phys. Rev. D **102**, 023004 (2020).
[44] A. Arvanitaki, S. Dimopoulos, M. Galanis, L. Lehner, J. O. Thompson, and K. Van Tilburg, Phys. Rev. D **101**, 083014 (2020).